Contents lists available at ScienceDirect

Ocean Engineering

journal homepage: www.elsevier.com/locate/oceaneng

Relationship between eroded volume and main scour hole dimensions near quay walls caused by internal counter-rotating twin-propellers

Giuseppe Curulli [a], Toni Llull [b,*], Nadia Penn [a], Anna Mujal-Colilles [c], Xavier Gironella [d], Agustin Sanchez-Arcilla [d], Roberto Gaudio [a]

[a] Dipartimento di Ingegneria Civile, Università della Calabria, 4 87036 Rende (CS), Italy
[b] Maritime Engineering Laboratory, Department of Nautical Science and Engineering, Universitat Politècnica de Catalunya BarcelonaTech (UPC), Barcelona, Spain
[c] Department of Nautical Science and Engineering, Universitat Politècnica de Catalunya BarcelonaTech (UPC), Barcelona, Spain
[d] Maritime Engineering Laboratory, Department of Civil and Environmental Engineering, Universitat Politècnica de Catalunya BarcelonaTech (UPC), Barcelona, Spain

ARTICLE INFO

Keywords:
Propeller-induced scour
Physical model
Harbour management
Eroded volumes

ABSTRACT

The present study aims at computing and analysing the eroded sediment volumes induced by twin-propeller jets near a vertical quay wall from the main geometric characteristics of the scour hole. Two different scouring mechanisms govern the scouring process: i) the down-flow due to the interaction between the propellers jet and the wall, and ii) the direct impact of the propellers jet flow on the seabed. For this reason, the whole study area is divided into two subzones: 1) 'near the wall' field; 2) 'far from the wall' field. Both forward and backward rotation of the propellers during manoeuvring are analysed. The results show that, for the two manoeuvring states, the relationship between the eroded volume and the geometric characteristics of the scour hole in the near-wall subzone does not change, meaning that the backward rotation does not affect the morphology of the scour hole near the wall. Moreover, the eroded volume can be determined as a function of the maximum depth near the wall and, with higher accuracy, as a product of the three main geometric characteristics of the scour hole at any time-stage during the scour hole development.

1. Introduction

The water jets generated by manoeuvring ship propellers in a harbour basin induce high hydrodynamic forces over the sediments and can generate a scour hole at the toe of the quay wall, compromising the stability of the structure (e.g., Lam et al., 2011; PIANC, 2015; Mujal-Colilles et al., 2017(a); Wei et al., 2018). The turbulent propeller jet flow reaches the seabed or is deflected by the quay structure of the harbour basin, leading to the development of one or more scour holes at the impingement location (Hamill et al., 1999; Yüksel et al., 2019). The scouring process goes hand in hand with the deposition of the scoured sediments, which can cause problems to the ship navigation, owing to the reduction of the water depth (e.g., Whitehouse, 1998; Sumer and Fredsoe, 2002; Gaythwaite, 2004; Abramowicz-Gerigk, 2010; Lam et al., 2011; Yew et al., 2017). Moreover, the dispersion of fine sediments into the water, as well as that of oil and fuel, can create non-negligible effects on the environment (e.g., Ji et al., 2014; Hong et al., 2016). Thus, the rotation of the ship propellers can induce important effects that must be considered in the design and maintenance of harbours basins.

In order to better understand the scouring mechanism, many researchers focused their studies on the estimation of the efflux velocity, i.e., the maximum value of the flow velocity downstream of the propeller plane (U_0) (e.g., Hamill et al., 2015; Hamill and Kee, 2016; Wei and Chiew, 2019) and its effects on the seabed (e.g., Hamill, 1988; Hamill et al., 1999; Hong et al., 2013; Tan and Yüksel, 2018; Penna et al., 2019). Once U_0 is known, the densimetric Froude number $F_0 = U_0/\sqrt{gd_{50}\Delta}$, which is considered by many researchers (e.g., Hamill et al., 1999; Tan and Yüksel, 2018; Penna et al., 2019) as the main parameter influencing the propeller scouring process, can be calculated, where g is the acceleration of gravity, d_{50} the median diameter of sediments, and $\Delta = (\rho_s - \rho)/\rho$ the relative submerged grain density, ρ_s and ρ being the sediment and fluid density, respectively.

The jet induced by a rotating propeller can occur in two different conditions, i.e., unconfined and confined conditions, as underlined by Wei et al. (2020), who recently published an extensive review about this

* Corresponding author.
E-mail addresses: giuseppe.curulli@unical.it (G. Curulli), antoni.llull.marroig@upc.edu (T. Llull), nadia.penna@unical.it (N. Penn), anna.mujal@upc.edu (A. Mujal-Colilles), xavi.gironella@upc.edu (X. Gironella), agustin.arcilla@upc.edu (A. Sanchez-Arcilla), roberto.gaudio@unical.it (R. Gaudio).

https://doi.org/10.1016/j.oceaneng.2022.111744
Received 31 January 2022; Received in revised form 8 May 2022; Accepted 11 June 2022

topic. The former is characterised by the absence of any type of confinement, whereas the latter includes the presence of a structural element in front of the propeller face interfering with the flow field and, hence, with the scouring process induced by the propeller. This is the case of a closed-type quay wall (i.e., a vertical solid wall) or an open-type quay wall (e.g., quay slab supported by a pile group, piled platforms, open berth quay; Sumer and Fredsoe, 2002; PIANC, 2015).

Many works concerning the study of the effects induced by a single rotating ship propeller in unconfined conditions are found in the literature. For instance, Hong et al. (2013) studied the temporal evolution of the longitudinal profiles of the scour hole and the deposition mound by underling their affinity for both the low and high propeller submergence conditions, whereas Tan and Yüksel (2018) proposed equations for the prediction of the geometric characteristics of the scour hole as a function of F_0. For the first time, Penna et al. (2019) proposed relationships between the eroded volume of sediments and the main geometric characteristics of the scour hole: maximum scour depth, maximum length evaluated along the centreline and maximum width. In confined conditions, Hamill et al. (1999) studied the confined scour hole due to a single rotating propeller and proposed an expression to estimate the change in maximum scour depth due to the confinement at the equilibrium state. Yüksel et al. (2019) compared the unconfined longitudinal scour profiles with those in confined conditions, when the confinement is due to a vertical wall (closed-type quay wall) at different time steps up to the equilibrium state, providing an equation for the estimation of the equilibrium scour depth near the quay wall. Instead, Wei and Chiew (2017), focusing their studies on the propeller scour in the presence of a sloping bank (open-type quay wall), showed how the distance between the propeller face and the structure influences the three main geometric characteristics of the scour hole.

Very few experimental studies on twin-propellers in confined conditions are found in literature. This propulsion system is generally associated with ferries, Ro-Ro and Ro-PAX ships, which do not usually need tug assistance therefore increasing the potential erosion consequences. Cui et al. (2020) and Llull et al. (2021) produced the most recent works on the topic. In the former, the maximum scour depth at the centreline was studied for a unique bed elevation, at different wall clearances. In the latter, the authors analysed the local scour due to confined twin-propellers in both forward and backward rotations, at four different combinations of wall and bed clearance distances, and proposed two temporal models to estimate the maximum scour depth from the experimental variables.

Nevertheless, few studies on scouring due to twin-propellers were found in the literature, in particular none concerning the quantification of the eroded sediment volumes in confined condition and its correlation with the other geometric characteristics of the scour hole. For this reason, the aim of this study is to evaluate the eroded sediment volumes (V_e) for internal counter-rotating twin-propellers, providing new formulae for the estimation of V_e as a function of the main geometric characteristics of the scour hole, i.e., the scour hole length, width and depth. Specifically, for the first time, scour data from two different manoeuvring states was used to compute and analyse V_e, named *Forward* (FWD) scenario when the propellers jet flow was constantly directed towards the quay structure and *Back&Forth* (B&F) scenario when the direction of the flow was alternated every 5 min. Methods to estimate the eroded volume could be valuable to account for the amount of sediment that is relocated owing to the vessel traffic in a harbour basin, allowing a better planning of the dredging operations to flat the basin and refill the induced holes. Thus, the present work represents a step forward in understanding the localized scour processes induced by twin-propellers in confined conditions.

2. Experimental tests

Experiments on local scour due to twin-propellers in confined conditions are presented. The data used to compute and analyse the eroded sediment volume were taken from Llull et al. (2021), who carried out a set of 24 experimental runs, where three rotational speeds (n), two bed clearances, i.e., the distance from the propeller axis to the sandy bed (C_h), and two wall distances from the propeller face (X_w) were tested. The tests were conducted in the Marine Engineering Laboratory at the *Universitat Politècnica de Catalunya* (UPC)-Barcelona Tech University, Catalunya, Spain, in a medium-scale water tank named *LaBassa* (see Fig. 1), filled in with a 0.7 m deep sand layer. Due to the common difficulties in sediment scaling, an effort was made in the selection and cleaning of the sediment by using the smallest and most uniform sediment present in the marker with $d_{50} = 0.25$ mm and $d_{90} = 0.375$ mm, where d_{50} and d_{90} are the 50% and 90% (by weight) finer sizes of sand, respectively. The tank was later filled in with fresh water up to a depth (h) of 0.7 m and, thus, emptied after each experiment. Before every new experiment, the sand bed was levelled and the tank was refilled carefully to avoid sediment resuspension and changes in the bed morphology. More detailed information about the tank can be found in Mujal-Colilles et al. (2017a, 2017b) and Mujal-Colilles et al. (2018).

In Fig. 2, a sketch of the scaled model of the two counter-rotating propellers used is shown. Each propeller had four blades ($N = 4$), an external propeller diameter (D_p) equal to 0.25 m, a hub diameter (D_h) of 2.5 cm and an Expanded Area Ratio (EAR) without hub (β) equal to 0.72, whereas the distance between the propeller axes (a_p) was set at 0.5 m. In particular, β was calculated as the ratio between the Total Blade Area (TBA) and the Propeller Disc Area (PDA): the former is defined as the product between N and the area of a single blade, whereas the latter is the area of a disk having the same diameter of the propeller. In Table 1 a summary of all the propeller characteristics is presented.

Before starting the experimental campaign, the time-averaged velocity distribution close to the propeller plane in unconfined conditions was measured. Thus, the thrust coefficient (c_t) was experimentally estimated using Eq. (1) proposed by Fuehrer and Romisch (1977) and assuming that U_0 is linearly dependent on n:

$$U_0 = 1.59 n D_p \sqrt{c_t} \tag{1}$$

Once c_t was obtained, U_0 was computed for each value of n and, then, F_0 was calculated, yielding values between 23 and 32.

To fulfil the similarity requirements, the Froude similarity law was used in the present work. However, Reynolds number requirements were also accounted to follow the guidelines of Verhey (1983). Thus, the Reynolds numbers of the flow [Re_f, Eq. (2)] and the Reynolds number of the propeller [Re_p, Eq. (3)] were set higher than $3{\cdot}10^3$ and $7{\cdot}10^4$, respectively:

$$Re_f = \frac{U_0 D_p}{\nu} \tag{2}$$

$$Re_p = \frac{n D_p L_m}{\nu} \tag{3}$$

In the previous expressions, ν is the kinematic viscosity of water (10^{-6} m^2 s^{-1} at a temperature of 20 °C) and L_m is the characteristic length expressed by Blaauw and van de Kaa (1978) as follows [Eq. (4)]:

$$L_m = \beta D_p \pi \left[2N \left(1 - \frac{D_h}{D_p} \right) \right]^{-1} \tag{4}$$

In the present work, the eroded volumes V_e due to both the FWD and B&F scenarios were analysed. In particular, FWD data was used to obtain new equations for the estimation of V_e by considering the main geometric characteristics of the scour holes, whereas B&F data was used to verify the replication of the results. The FWD tests were performed with a constant propeller rotation directed towards the wall (forward rotation), whereas in the B&F tests the propeller rotation changed intermittently every 5 min, starting from backward rotation. The total duration (t_d) of each test was set to 30 min and the bed surface was scanned every 5 min to observe the evolution of the scouring process. When the propellers were close to the bottom (i.e., with the minimum

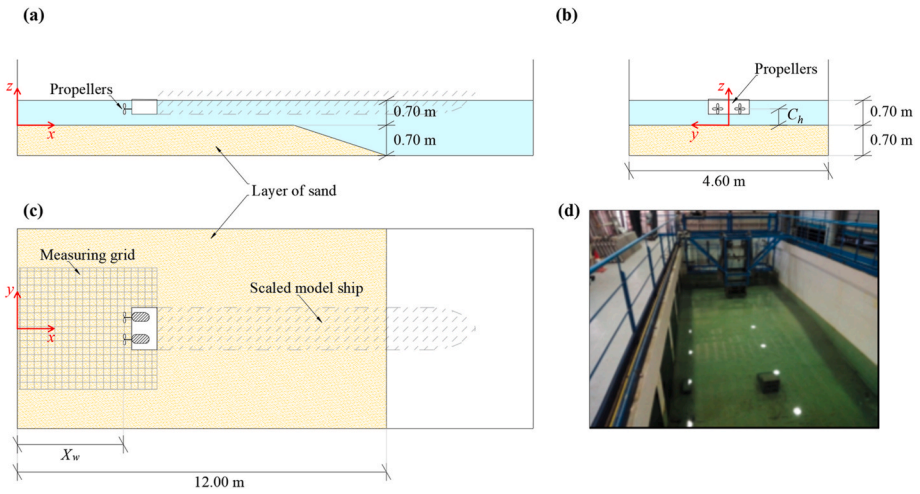

Fig. 1. Out-of-scale sketch of the experimental installation [(a) lateral, (b) transversal and (c) plan view] and (d) picture of the experimental installation.

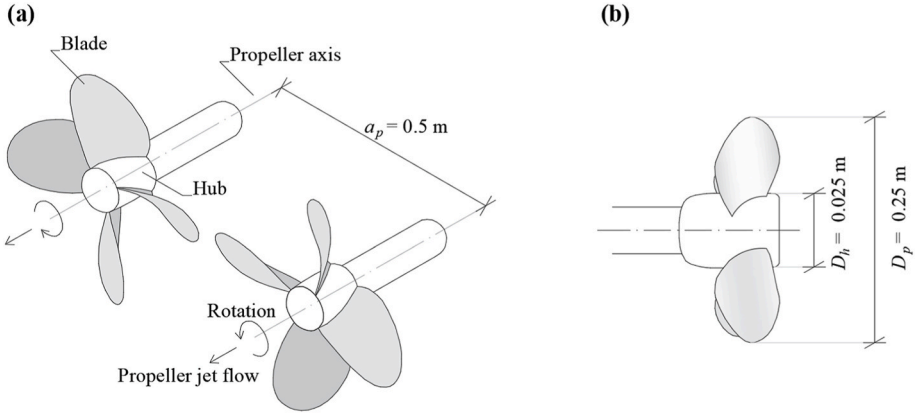

Fig. 2. Out-of-scale (a) sketch of the counter-rotating twin-propellers and (b) lateral view of a single propeller.

Table 1
Characteristics of a single propeller.

Propeller diameter, D_p (m)	0.25
Hub diameter, D_h (cm)	2.5
Number of blades, N	4
Expanded Area Ratio (EAR) without hub, β	0.75
Thrust coefficient, c_t	0.65

bed clearance), especially for high values of n, the experiments were extended up to 60 min to observe the further evolution of the scour holes.

Table 2 shows a recap of the experimental conditions of the tests: in the following, the minimum and maximum values of C_h and X_w will be indicated as $C_{h,\min}$, $C_{h,\max}$, $X_{w,\min}$ and $X_{w,\max}$, respectively.

As stated by Hamill (1987) and Hong et al. (2013), the effect on the overall scour of switching the propellers rotation on and off can be neglected. Thus, the propellers were stopped and started at each time interval to allow the bed scanning, which was performed by two UltraLab UWS1M Echo Sounders with an accuracy of 1%.

The adopted reference system was composed of three mutually orthogonal axes: the origin of the streamwise axis (x) was set in correspondence of the quay wall, that of the spanwise axis (y, directed from the left to the right side of the tank looking downstream towards the wall) was set in correspondence of the central axis between the two propellers, whereas the origin of the vertical axis (z) was set in correspondence of the undisturbed bed surface at the beginning of each test.

Table 2
Experimental conditions of the tests carried out by Llull et al. (2021). Experiments highlighted in blue were extended up to 60 min.

No.	t_d (s)	n (rpm)	C_h (m)	X_w (m)	Scenario
1	1800	300	0.250	1.75	FWD
2	1800	350			
3	3600	400			
4	1800	300	0.375		
5	1800	350			
6	1800	400			
7	1800	300	0.250	2.50	
8	1800	350			
9	1800	400			
10	1800	300	0.375		
11	1800	350			
12	1800	400			
13	1800	300	0.250	1.75	B&F
14	1800	350			
15	1800	400			
16	1800	300	0.375		
17	1800	350			
18	1800	400			
19	3600	300	0.250	2.50	
20	3600	350			
21	3600	400			
22	1800	300	0.375		
23	1800	350			
24	1800	400			

The bed elevation grids, each consisting of 372 points along x and 150 points along y, with a spatial resolution (Δx and Δy) of 1.00 and 1.75 cm, respectively, were used in the present work to evaluate the eroded sediment volumes, as shown in the following section.

More details on the experimental procedure can be found in Llull et al. (2021).

3. Methods

For each experimental test, the negative bed elevation data (z) refers to the eroded areas of the bed surfaces. By considering z as a function of the two variables x and y, V_e was evaluated through the double integration of the grid along x and y. In particular, since the analytical function $z = f(x, y)$ is unknown, the trapezoidal numerical integration was implemented in *MATLAB*® environment according to the formula:

$$V_e = \int_x \int_y z(x,y)dxdy \approx \frac{\Delta x}{2} \sum_{j=1}^{k_1-1} \frac{\Delta y}{2} \sum_{i=1}^{k_2-1} \left(z_{i,j} - z_{i+1,j+1}\right) \quad (5)$$

where $i = 1, 2, 3, \ldots, k_1-1$; k_1 is the number of elements along the x axis; $j = 1, 2, 3, \ldots, k_2-1$; and k_2 is the number of elements along the y axis, across the whole measuring grid.

The FWD scenario is characterised by the presence of three scour holes: the first one is formed immediately downstream of the propeller face; the second one is due to the interaction between the propellers' jet flow and the quay structure; the third one (named small scour hole) can be found behind the propellers [Yüksel et al., 2019; Llull et al., 2021; see Fig. 3(a)].

In the B&F scenario, two or three scour holes are visible: one upstream of the propellers face due to the backward rotation, one at the toe of the quay wall caused by the deflected jet in forward rotation, whereas an additional scour hole between them was observed in some cases [see Fig. 3(b)]. This latter scour hole is due to the propeller jet flow that directly impacts the sandy bottom when the forward rotation occurs (Llull et al., 2021).

In this work, the whole study area was divided into two planar subzones, 'near the wall' field (nw) and 'far from the wall' field (fw): the first only includes the scour hole near the wall for both the FWD and B&F scenarios, whereas the second comprises the small and the main scour holes in the FWD scenario. B&F data was used to validate only the results obtained in the near-wall hole, since the effects of the backward rotation are not present in this subzone, so that the scour hole development is comparable for both regimes.

The aim of the present analysis is to express $V_e = V_{e,nw} + V_{e,fw}$ in the FWD scenario as a function of the geometric characteristics of the scour holes, which are the maximum scour depths of the scour holes at the centreline ($d_{sc,nw}$ and $d_{sc,fw}$), their maximum lengths along the centreline ($l_{sc,nw}$ and $l_{sc,fw}$) and their maximum widths ($b_{s,nw}$ and $b_{s,fw}$) evaluated at the location of $d_{sc,nw}$ and $d_{sc,fw}$, respectively.

The centreline longitudinal scour profiles were used to locate the separation point between the near-wall subzone and that far from the quay structure. For each test, the separation point between the two subzones was found by locating the first local maximum of the centreline longitudinal profile closest to the wall (Llull et al., 2021), as reported in Fig. 4(a). When the first local maximum cannot be found, owing to the merging of the two scour holes, the point of minimum curvature of the centreline longitudinal profile closest to the wall was considered as the separation between the two subzones, as shown Fig. 4(b). The separation points where symbolised with open dots in Fig. 4.

The length of the scour hole near the wall, $l_{sc,nw}$, was defined as the distance between the quay structure and the first up-crossing zero of the longitudinal profile near the wall (by going towards the propeller face). On the other hand, the length of the scour hole far from the wall, $l_{sc,fw}$, was defined as the distance between the first down-crossing zero of the longitudinal profile and the local maximum closest to the propeller face [see Fig. 5(a)]. When the separation point had negative elevation, $l_{sc,nw}$ was evaluated as the distance between this point and the wall, whereas $l_{sc,fw}$ was equal to the distance between the separation point and the local maximum closest to the propellers face [see Fig. 5(b)]. Moreover, $b_{s,nw}$ and $b_{s,fw}$ were evaluated as the distance along the y direction between the two internal zero-crossing points of the transverse scour profiles in correspondence of $d_{sc,nw}$ and $d_{sc,fw}$, respectively. An example is reported in Fig. 6 for better guidance, which shows the transversal scour profile at the location of $d_{sc,fw}$ for $C_{h,\min}$, $X_{w,\min}$, $n = 300$ rpm and $t = 30$ min.

The same procedures were used in the B&F scenario to recognise the two subzones and evaluate the geometric characteristics of the scour hole near the wall.

In the FWD scenario, Llull et al. (2021) and Mujal-Colilles et al. (2018) observed that a reduction in C_h induces a deeper scour hole far from the wall, whereas the scour near the quay wall is mostly influenced by X_w, as stated by Llull et al. (2021). For this reason, $V_{e,nw}$, $d_{sc,nw}$, $l_{sc,nw}$ and $b_{s,nw}$ were made dimensionless by dividing by X_w^3 or X_w, respectively ($V_{e,nw}/X_w^3$, $d_{sc,nw}/X_w$, $l_{sc,nw}/X_w$ and $b_{s,nw}/X_w$), whereas $V_{e,fw}$, $d_{sc,fw}$, $l_{sc,fw}$ and $b_{s,fw}$ were made dimensionless by dividing by C_h^3 or C_h, respectively ($V_{e,fw}/C_h^3$, $d_{sc,fw}/C_h$, $l_{sc,fw}/C_h$ and $b_{s,fw}/C_h$). On the contrary, D_p^3 was used to make V_e dimensionless, because this latter is influenced by both C_h and X_w, without prevalence of anyone of them.

4. Discussion and results

Penna et al. (2019) proposed three different equations to estimate the total eroded volume in unconfined conditions as a function of the main geometric characteristics of the scour hole owing to a single rotating propeller: dimensionless total eroded volume (V_e/D_p^3) versus dimensionless absolute maximum scour depth (d_s/D_p), dimensionless maximum scour length evaluated along the centreline (l_{sc}/D_p), and dimensionless maximum scour width evaluated in correspondence of d_s (b_s/D_p), respectively.

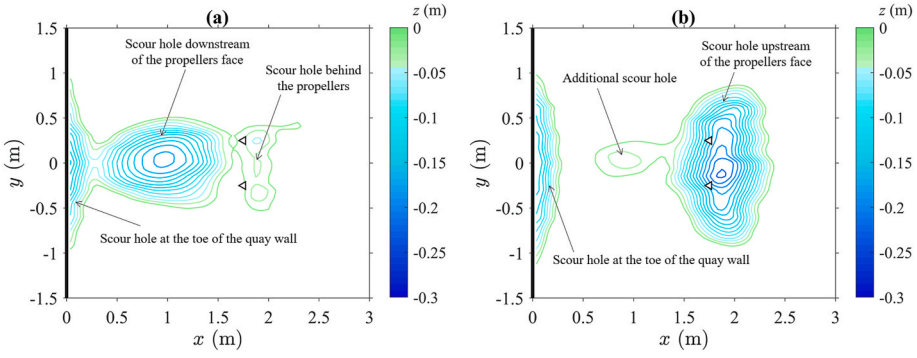

Fig. 3. Contour plot of the three scour holes due to confined counter-rotating twin-propellers for $C_{h,\min}$, $X_{w,\min}$, $n = 300$ rpm and $t = 30$ min in (a) the FWD scenario and (b) the B&F scenario. The triangles represent the position of the propellers in the x-y plane.

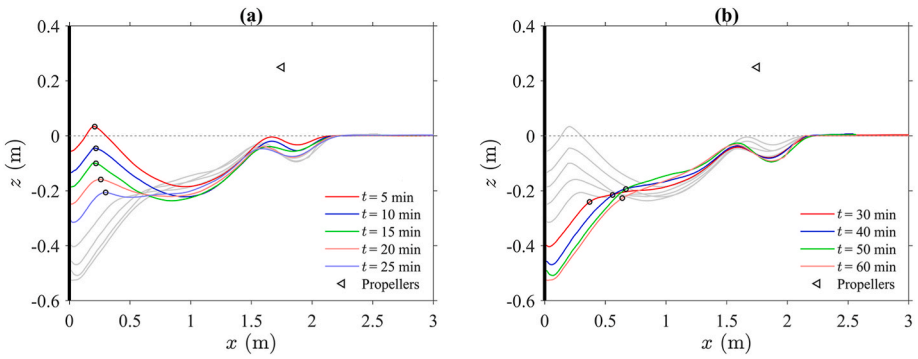

Fig. 4. Time evolution of the centreline longitudinal scour profiles for $C_{h,\min}$, $X_{w,\min}$ and $n = 400$ rpm in the FWD scenario. The open dots represent the separation points between the near-wall subzone and that far from the structure. The separation is (a) the local maximum closest to the wall for no-merged scour holes and (b) the point of minimum curvature closest to the wall for merged scour holes. The triangles represent the position of the propellers in the *x*-*z* plane.

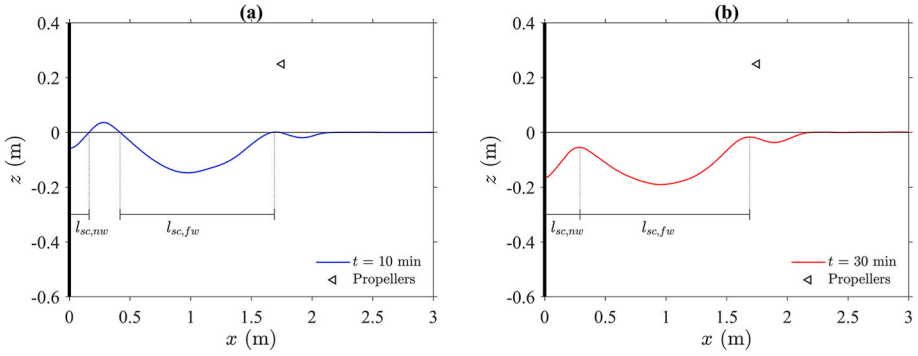

Fig. 5. Centreline longitudinal scour profile for (a) $C_{h,\min}$, $X_{w,\min}$, $n = 300$ rpm and $t = 10$ min, and (b) $C_{h,\min}$, $X_{w,\min}$, $n = 300$ rpm and $t = 30$ min, in the FWD scenario. The triangle represents the position of the propellers in the *x*-*z* plane.

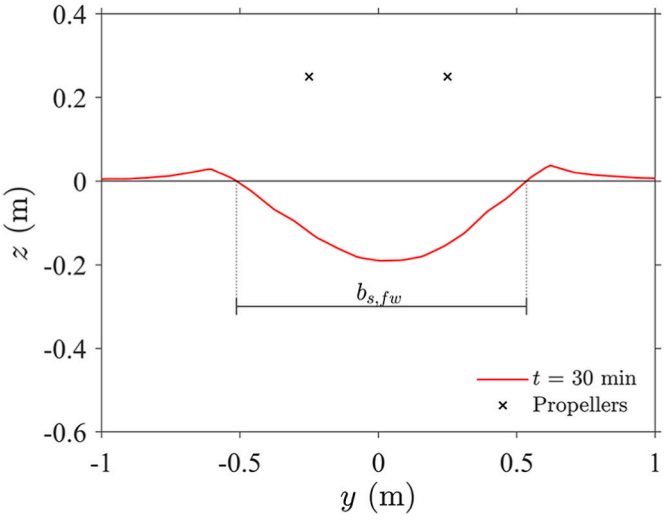

Fig. 6. Transversal scour profile at the location of $d_{sc,fw}$ for $C_{h,\min}$, $X_{w,\min}$, $n = 300$ rpm and $t = 30$ min, in the FWD scenario. The cross-dots represent the position of the propellers in the *y*-*z* plane, looking downstream towards the wall.

In the case of confined counter-rotating twin-propellers, the maximum scour depths at the centreline were considered instead of the absolute maximum scour depth, by committing a negligible error, as stated by Llull et al. (2021). However, in the FWD scenario, the geometric characteristics of the scour hole near the quay wall are not comparable with those evaluated in the subzone far from the structure. In particular, the scour hole near the wall appears to be elongated in the spanwise direction, because of the laterally deflected flow owing to the wall obstruction; in fact, $b_{s,nw} > b_{s,fw}$ for any value of X_w, C_h, n and t. In most of the cases, $l_{sc,nw}$ is less than $l_{sc,fw}$, with exceptions in some particular merged scour holes ($X_{w,\min}$, $C_{h,\max}$, $n = 400$ rpm and $t > 15$ min). This is due to the fact that the erosive force of the wall-deflected propeller jet flow, acting for long time, induces a deeper and longer scour hole near the wall, whereas an increase in C_h induces a reduction in $l_{sc,fw}$. In addition, $d_{sc,nw}$ is always greater than $d_{sc,fw}$ for $C_{h,\max}$. Consequently, the absolute maximum scour depth at the centreline (with no consideration of the two subzones), d_{sc}, is found near the quay wall ($d_{sc} = d_{sc,nw}$). Differently, for $C_{h,\min}$, the position of d_{sc} depends on n and t: d_{sc} is equal to $d_{sc,nw}$ only for $n = 400$ rpm and $t > 20$ min, otherwise d_{sc} is found in the far-from-the-wall subzone.

Given all, it is reasonable to assume that the eroded volumes in the two subzones depend on the geometric characteristics (hereinafter named geometric dimensions) of each scour hole, by considering each of them independent from the other.

Aiming at obtaining simple equations to estimate the eroded volume from a single variable, its dependency on the scour length, width and depth in each subzone was studied at any arbitrary time-stage of the scour development. In the following, the determination coefficient (R^2) and a mean relative error (E_r) are used to verify the goodness of the proposed formulae. In particular, E_r was evaluated as follows, as reported by Coscarella et al. (2020) [Eq. (6)]:

$$E_r = \frac{1}{N_0}\sum_{k=1}^{N_0}\frac{|v_{m,k} - v_{c,k}|}{v_{m,k}} \tag{6}$$

where $k = 1, 2, 3, \ldots, N_0$, N_0 is the number of analysed data, $v_{m,k}$ is the kth measured value of the eroded volume ($V_{e,nw}/X_w^3$, $V_{e,fw}/C_h^3$ or V_e/D_p),

whereas $v_{c,k}$ is the correspondent computed value.

The relation between the eroded volumes and the scour lengths or the scour widths are not very clear [see Fig. 7(a–d), for $V_{e,nw}/X_w^3$ vs. $l_{sc,nw}/X_w$, $V_{e,fw}/C_h^3$ vs. $l_{sc,fw}/C_h$, $V_{e,nw}/X_w^3$ vs. $b_{s,nw}/X_w$, and $V_{e,fw}/C_h^3$ vs. $b_{s,fw}/C_h$, respectively], whereas the relationships between the eroded volumes and the maximum scour depth at the centreline in each subzone follow Eqs. (7) and (8) for the near-wall and far-from-the-wall subzones, respectively [see Fig. 8(a–b), for $V_{e,nw}/X_w^3$ against $d_{sc,nw}/X_w$ and for $V_{e,fw}/C_h^3$ against $d_{sc,fw}/C_h$, respectively]. Therefore, the experimental results show that the eroded volume, in case of confined propeller jets, can be estimated from measurements of the longitudinal central bed profile, at any time during the scour process:

$$\frac{V_{e,nw}}{X_w^3} = 1.20\left(\frac{d_{sc,nw}}{X_w}\right)^{2.11} \tag{7}$$

$$\frac{V_{e,fw}}{C_h^3} = 15.71\left(\frac{d_{sc,fw}}{C_h}\right)^{2.20} \tag{8}$$

The R^2 are equal to 0.93 and 0.92, whereas the E_r are equal to 29% and 39%, for Eqs. (7) and (8), respectively.

In order to improve the agreement of the data to Eqs. (7) and (8) and reasonably assuming that the eroded volumes depend on the three geometric dimensions of the scour holes, the products of these quantities were considered as independent variables.

In particular, two formulae, one for each subzone, were proposed: Fig. 9(a) shows the relationship between $d_{s,nw}{\cdot}l_{sc,nw}{\cdot}b_{s,nw}/X_w^3$ and $V_{e,nw}/X_w^3$ [Eq. (9)], whereas in Fig. 9(b) the same formula was applied to the B&F data to discuss the replication of the results; instead, Fig. 10 shows the relationship between $d_{s,fw}{\cdot}l_{sc,fw}{\cdot}b_{s,fw}/C_h^3$ and $V_{e,fw}/C_h^3$ [Eq. (10)]:

$$\frac{V_{e,nw}}{X_w^3} = 0.57\left(\frac{d_{sc,nw}\cdot l_{sc,nw}\cdot b_{s,nw}}{X_w^3}\right)^{1.18} \tag{9}$$

$$\frac{V_{e,fw}}{C_h^3} = 0.43\left(\frac{d_{sc,fw}\cdot l_{sc,fw}\cdot b_{s,fw}}{C_h^3}\right) \tag{10}$$

The R^2 coefficients are equal to 0.98 and 0.95, whereas the relative errors E_r are equal to 23% and 18%, for Eqs. (9) and (10), respectively. In particular, for the replication of the results in the B&F scenario, $R^2 = 0.96$ and $E_r = 23\%$, proving that Eq. (9) could also be used for the computation of $V_{e,nw}/X_w^3$ in the B&F scenario.

In the previous expressions, if Eqs. (7) and (8) are replaced with Eqs. (9) and (10), the power law exponents become smaller, as well as the coefficients. In particular, the exponent of Eq. (9) is very close to one, whereas Eq. (10) is practically a linear law. Moreover, the R^2 coefficients become greater and the E_r smaller, when using $d_{s,nw}{\cdot}l_{sc,nw}{\cdot}b_{s,nw}/X_w^3$ and $d_{s,fw}{\cdot}l_{sc,fw}{\cdot}b_{s,fw}/C_h^3$ instead of $d_{s,nw}/X_w$ and $d_{s,fw}/C_h$, respectively.

Also, by summing the two products $(V_{e,nw}/X_w^3){\cdot}(X_w^3/D_p^3)$ and $(V_{e,fw}/C_h^3){\cdot}(C_h^3/D_p^3)$, where $V_{e,nw}/X_w^3$ and $V_{e,fw}/C_h^3$ were calculated with Eqs. (9) and (10), respectively, it was possible to provide another equation to evaluate V_e/D_p^3 [Eq. (11)], as reported in Fig. 11:

$$\frac{V_e}{D_p^3} = \left(\frac{V_{e,nw}}{X_w^3}\right)_{\text{eq.9}}\frac{X_w^3}{D_p^3} + \left(\frac{V_{e,fw}}{C_h^3}\right)_{\text{eq.10}}\frac{C_h^3}{D_p^3} \tag{11}$$

The R^2 coefficient is equal to 0.97, whereas the E_r is equal to 11%. The agreement between Eq. (11) and the data, in the FWD scenario, can be also considered as a further confirmation of the robustness of Eqs. (9) and (10). The existence of two different scour holes is the main reason behind the separate computation of the eroded volume in the sub-areas, because each scour hole is caused by a different mechanism, as previously explained.

The aforementioned expressions [from Eq. (7) to Eq. (10)] show different methods for estimating the total eroded volume due to a confined twin propeller model in the range of the experimental variables used in the study. They also provide evidence on the need to approach this problem from a three-dimensional perspective. The consistent relation between the different geometric characteristics and the total eroded volume suggests that the total removed material is not conditioned by the physical boundaries. Also a limited expansion in one of the three spatial dimensions - as in the case of the vertical wall - is always compensated by an increase along the other directions, since the total

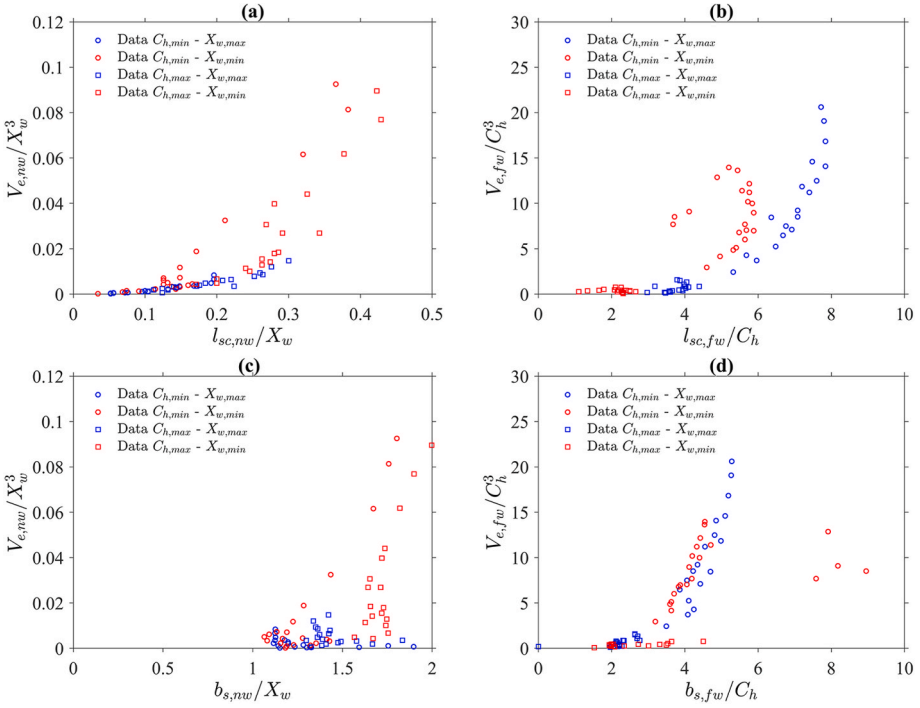

Fig. 7. Dimensionless eroded volume in the near-wall subzone ($V_{e,nw}/X_w^3$) vs. (a) the dimensionless maximum scour length, $l_{sc,nw}/X_w$, and (c) the dimensionless maximum scour width, $b_{s,nw}/X_w$, in the FWD scenario; dimensionless eroded volume in the far-from-the-wall subzone ($V_{e,fw}/C_h^3$) vs. (b) the dimensionless maximum scour length, $l_{sc,fw}/C_h$, and (d) the dimensionless maximum scour width, $b_{s,fw}/C_h$, in the FWD scenario.

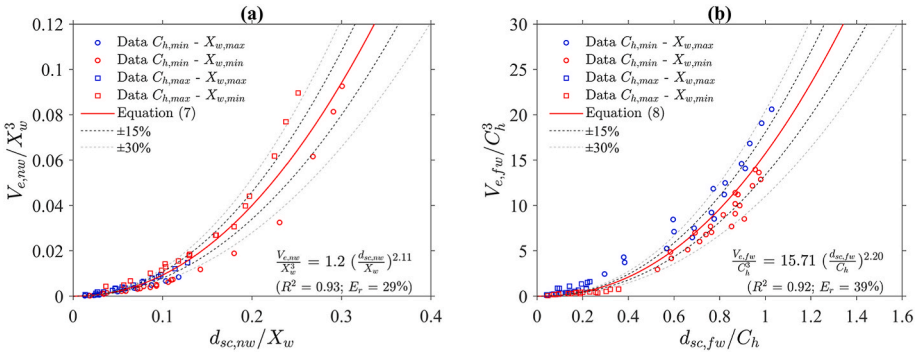

Fig. 8. Dimensionless eroded volume in (a) the near-wall subzone ($V_{e,nw}/X_w^3$) vs. the dimensionless maximum scour depth, $d_{sc,nw}/X_w$, and (b) the far-from-the-wall subzone ($V_{e,fw}/C_h^3$) vs. the dimensionless maximum scour depth, $d_{sc,fw}/C_h$, in the FWD scenario. The red solid lines represent Eqs. (7) and (8), which are also reported in the figure, whereas the dashed lines represent the associated ±15% and ±30% error bounds.

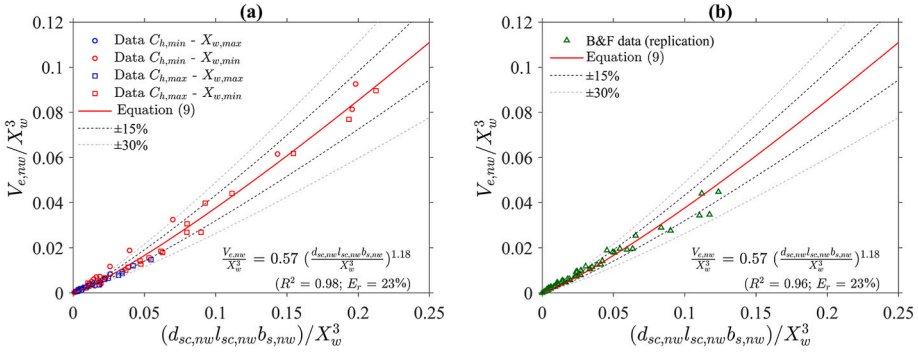

Fig. 9. Dimensionless eroded volume in the near-wall subzone ($V_{e,nw}/X_w^3$) vs. the product of the three main geometric dimensions of the scour hole near the wall (maximum scour depth, $d_{sc,nw}$, maximum scour length, $l_{sc,nw}$, and maximum scour width, $b_{s,nw}$) in (a) the FWD scenario, and (b) the B&F scenario. The red solid lines represent Eq. (9), which is also reported in the figure, whereas the dashed lines represent the associated ±15% and ±30% error bounds.

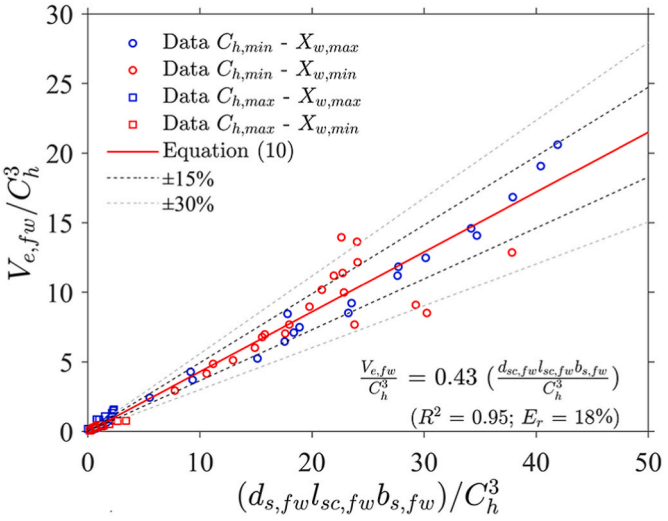

Fig. 10. Dimensionless eroded volume in the far-from-the-wall subzone ($V_{e,fw}/C_h^3$) vs. the product of the three main geometric dimensions of the scour hole far from the wall (maximum scour depth, $d_{sc,fw}$, maximum scour length, $l_{sc,fw}$, and maximum scour width, $b_{s,fw}$). The red solid line represents Eq. (10), which is also reported in the figure, whereas the dashed lines represent the associated ±15% and ±30% error bounds.

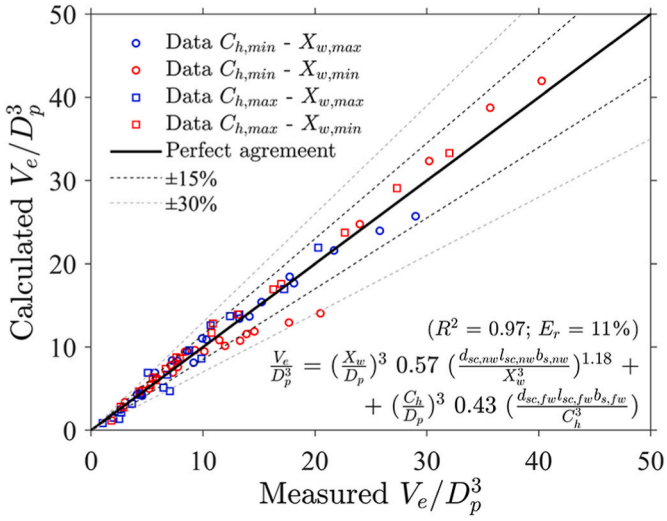

Fig. 11. Comparison between measured V_e/D_p^3 and calculated V_e/D_p^3 with Eq. (11). The black solid line represents the perfect agreement between measured and calculated values with Eq. (11), which is also reported in the figure, whereas the dashed lines represent the associated ±15% and ±30% error bounds.

amount of material eroded is maintained constant. These assumptions need to be verified with further experimental researches, which should include a wider range of combinations of the most relevant variables investigated in this work.

5. Conclusions

The total eroded volume (V_e) due to confined twin-propellers, in the FWD and B&F scenarios, have been analysed. A new relationship between total eroded volume and scour hole dimensions induced by twin

propellers has been presented and discussed.

The geometric characteristics of the scour holes, as well as the V_e, are divided into two subzones as follows: 'near the quay wall field' (nw) and 'far from the wall field' (fw). This subdivision was necessary because two different scour mechanisms occur in confined conditions: i) the direct interaction between the propeller jet flow and the vertical structure is responsible of the scour hole near the quay wall (Yüksel et al., 2019; Llull et al., 2021), whereas ii) the flow that collides with the sandy bottom determines the scour hole in front of the propellers (Llull et al., 2021). Then, the eroded volumes ($V_{e,nw}$ and $V_{e,fw}$), the maximum centreline scour depths ($d_{sc,nw}$ and $d_{sc,fw}$), the maximum centreline scour lengths ($l_{sc,nw}$ and $l_{sc,fw}$), and the maximum scour widths at the maximum depth location ($b_{s,nw}$ and $b_{s,fw}$), for both the two subzones, have been evaluated and discussed.

In the case of the confined twin-propellers, poor correlation was found between $V_{e,nw}/X_w^3$ and $l_{sc,nw}/X_w$ or $b_{s,nw}/X_w$ and between $V_{e,fw}/C_h^3$ and $l_{sc,fw}/C_h$ or $b_{s,fw}/C_h$. Instead, by expressing $V_{e,nw}/X_w^3$ and $V_{e,fw}/C_h^3$ as functions of $d_{sc,nw}/X_w$ and $d_{sc,fw}/C_h$, respectively, good agreements between the results of the proposed formulae and the experimental data were found, which increase by considering the products among the three dimensionless dimensions of each scour hole ($d_{s,nw}{\cdot}l_{sc,nw}{\cdot}b_{s,nw}/X_w^3$ and $d_{s,fw}{\cdot}l_{sc,fw}{\cdot}b_{s,fw}/C_h^3$) instead of $d_{sc,nw}/X_w$ and $d_{sc,fw}/C_h$, respectively.

The proposed formula for the calculation of $V_{e,nw}/X_w^3$ in the FWD scenario, as a function of $d_{s,nw}{\cdot}l_{sc,nw}{\cdot}b_{s,nw}/X_w^3$, returns satisfactory results also in the B&F scenario, proving that the scour hole near the wall is due to the deflected propeller jet flow without substantial additional sediment deposition, that could be caused by the alternation in the rotation of the propellers.

Summing the two proposed equations for $V_{e,nw}/X_w^3$ and $V_{e,fw}/C_h^3$, another formula is provided for evaluating V_e, made dimensionless by dividing by the cube of the propeller diameter (D_p^3).

The analysed relationships among the eroded volumes and the main scour holes geometric characteristics provide a reference model for researchers and engineers to calculate $V_{e,nw}$, $V_{e,fw}$ and V_e, by measuring $d_{s,nw}$, $l_{sc,nw}$, $b_{s,nw}$, $d_{s,fw}$, $l_{sc,fw}$ and $b_{s,fw}$ either in laboratory tests or in the field. The proposed formulae are not direct functions of the setup parameters (C_h, X_w, n) and time (t); however, their influence is already considered inside the geometric dimensions of the scour holes and the corresponding eroded volumes.

The validity of the proposed formulae is to be considered in the ranges of C_h, X_w and n here analysed and for $d_{s,nw}{\cdot}l_{sc,nw}{\cdot}b_{s,nw}/X_w^3 < 0.25$ and $d_{s,fw}{\cdot}l_{sc,fw}{\cdot}b_{s,fw}/C_h^3 < 45$, which were measured in the present work. In order to generalise the equations, a larger number of additional experiments should be performed with untested values of C_h, X_w and n. The geometric characteristics can evolve with time, following different patterns, by reaching separately the equilibrium state. However, further research is needed to extend the validity of the proposed equations until the equilibrium state is reached.

Funding

This work was supported by the Italian "*Programma Operativo Regione (POR) Calabria FESR-FSE 2014/2020*". TLL and AMC acknowledge the Agency for Management of University and Research Grants (AGAUR) and the Serra Húnter Programme of the *Generalitat de Catalunya*, respectively.

CRediT authorship contribution statement

Giuseppe Curulli: Investigation, Methodology, Formal analysis, Writing – original draft, Writing - revisions. **Toni Llull:** Conceptualization, Experimental work, Formal analysis, Writing – original draft. **Nadia Penn:** Investigation, Writing – original draft, Supervision. **Anna Mujal-Colilles:** Conceptualization, Investigation, Writing – original draft, Supervision. **Xavier Gironella:** Conceptualization, Resources, Writing – original draft, Project administration, Funding acquisition. **Agustin Sanchez-Arcilla:** Resources, Writing – original draft, Funding acquisition. **Roberto Gaudio:** Resources, Writing – original draft, Supervision, Project administration, Funding acquisition.

Declaration of competing interest

The authors declare that they have no known competing financial interests or personal relationships that could have appeared to influence the work reported in this paper.

Acknowledgements

We greatly acknowledge the technical staff of the UPC CIEMLAB for their support throughout the experimental work: Joaquim Sospedra, Òscar Galego and Ricardo Torres. AMC acknowledges the Serra Húnter Programme from the Generalitat de Catalunya.

Nomenclature

b_s	maximum scour width in unconfined conditions, m
$b_{s,fw}$	maximum scour width in the far-from-the-wall subzone, m
$b_{s,nw}$	maximum scour width in the near-wall subzone, m
C_h	propeller submergence depth, m
c_t	thrust coefficient
d_{50}	median diameter of bed sediments, m
d_s	absolute maximum scour depth in unconfined conditions, m
d_{sc}	absolute maximum scour depth at the centreline without considering the subdivision in two subzones, m
$d_{sc,fw}$	maximum scour depth in the far-from-the-wall subzone at the centreline in confined conditions, m
$d_{sc,nw}$	maximum scour depth in the near-wall subzone at the centreline in confined conditions, m
D_h	propeller hub diameter, m
D_p	external propeller diameter, m
E_r	mean relative error
F_0	densimetric Froude number
g	acceleration of gravity, m s^{-2}
h	water depth, m
L_m	propeller characteristic length, m
l_{sc}	maximum scour length in unconfined conditions, m
$l_{sc,fw}$	length of the scour hole far from the wall in confined conditions, m
$l_{sc,nw}$	length of the scour hole near the wall in confined conditions, m
n	rotational speed of the propeller, rpm
N	number of propeller blades
N_0	number of analysed data
PDA	propeller disc area, m^2
R^2	determination coefficient
Re_f	Reynolds number of the flow
Re_p	propeller Reynolds number
TBA	total blade area of the propeller, m^2
U_0	efflux velocity of the propeller flow, m s^{-1}
V_e	total eroded volume, m^3
$V_{e,fw}$	eroded volume in the far-from-the-wall subzone, m^3
$V_{e,nw}$	eroded volume in the near-wall subzone, m^3
X_w	distance between the quay wall and the propeller face, m

Greek symbols

β	expanded area ratio without hub
Δ	relative submerged grain density
ν	kinematic viscosity of water, m^2 s^{-1}
ρ	fluid density, kg m^{-3}
ρ_s	sediment density, kg m^{-3}

References

Abramowicz-Gerigk, T., 2010. Distribution of Flow Velocity Generated by Propellers of Twin Propeller Vessel. Zeszyty Naukowe/Akademia Morska w Szczecinie, pp. 5–12.

Blaauw, H.G., van de Kaa, E.J., 1978. Erosion of bottom and sloping banks caused by screw race of manoeuvring ships. In: 7th International Harbour Congress Antwerp. Delft Hydraulics Laboratory. May 22-26, 1978.

Coscarella, F., Gaudio, R., Manes, C., 2020. Near-bed eddy scales and clear-water local scouring around vertical cylinders. J. Hydraul. Res. 58 (6), 968–981.

Cui, Y., Lam, W.H., Ong, Z.C., Ling, L., Siow, C.L., Robinson, D., Hamill, G., 2020. Experimental scours by impinging twin-propeller jets at quay wall. J. Mar. Sci. Eng. 8 (11), 872.

Fuehrer, M., Romisch, K., 1977. Effects of modern ship traffic on islands and ocean waterways and their structures. In: PIANC 24th Congress, pp. 1–3.

Gaythwaite, J.W., 2004. Design of Marine Facilities for the Berthing, Mooring, and Repair of Vessels. American Society of Civil Engineers.

Hamill, G., 1987. Characteristics of the Screw Wash of a Manoeuvring Ship and the Resulting Bed Scour. Doctoral dissertation. Queen's University of Belfast.

Hamill, G.A., 1988. The scouring action of the propeller jet produced by a slowly manoeuvring ship. Bull. Perm. Int. Assoc. Navig. Congr. 62.

Hamill, G.A., Johnston, H.T., Stewart, D.P., 1999. Propeller wash scour near quay walls. J. Waterw. Port, Coast. Ocean Eng. 125 (4), 170–175.

Hamill, G.A., Kee, C., 2016. Predicting axial velocity profiles within a diffusing marine propeller jet. Ocean. Eng. 124, 104–112.

Hamill, G., Kee, C., Ryan, D., 2015. Three-dimension efflux velocity characteristics of marine propeller jets, 2. In: Proceedings of the Institution of Civil Engineers-Maritime Engineering, vol. 168. Thomas Telford Ltd, pp. 62–75.

Hong, J.H., Chiew, Y.M., Cheng, N.S., 2013. Scour caused by a propeller jet. J. Hydraul. Eng. 139 (9), 1003–1012.

Hong, J.H., Chiew, Y.M., Hsieh, S.C., Cheng, N.S., Yeh, P.H., 2016. Propeller jet-induced suspended-sediment concentration. J. Hydraul. Eng. 142 (4), 04015064.

Ji, S., Ouahsine, A., Smaoui, H., Sergent, P., 2014. 3D Numerical modeling of Sediment resuspension induced by the compounding effects of ship-generated waves and the ship propeller. J. Eng. Mech. 140 (6), 04014034.

Lam, W.H., Hamill, G.A., Song, Y.C., Robinson, D.J., Raghunathan, S., 2011. A review of the equations used to predict the velocity distribution within a ship's propeller jet. Ocean. Eng. 38 (1), 1–10.

Llull, T., Mujal-Colilles, A., Gironella, X., 2021. Twin propeller time-dependent scouring processes. Physical experiments. Ocean. Eng. 236, 109461.

Mujal-Colilles, A., Castells, M., Llull, T., Gironella, X., Martínez de Osés, X., 2018. Stern twin-propeller effects on harbor infrastructures. Experimental analysis. Water 10 (11), 1571.

Mujal-Colilles, A., Gironella, X., Crespo, A.J.C., Sanchez-Arcilla, A., 2017a. Study of the bed velocity induced by twin propellers. J. Waterw. Port, Coast. Ocean Eng. 143 (5), 04017013.

Mujal-Colilles, A., Gironella, X., Sanchez-Arcilla, A., Puig Polo, C., Garcia-Leon, M., 2017b. Erosion caused by propeller jets in a low energy harbour basin. J. Hydraul. Res. 55 (1), 121–128.

Penna, N., D'Alessandro, F., Gaudio, R., Tomasicchio, G.R., 2019. Three-dimensional analysis of local scouring induced by a rotating ship propeller. Ocean. Eng. 188, 106294.

PIANC (Permanent International Association of Navigation Congresses), 2015. Guidelines for protecting berthing structures from scour caused by ships. Rep. No. 180.

Sumer, B.M., Fredsoe, J., 2002. The Mechanics of Scour in the Marine Environment. World Scientific Publisher.

Tan, R.İ., Yüksel, Y., 2018. Seabed scour induced by a propeller jet. Ocean. Eng. 160, 132–142.

Verhey, H., 1983. The stability of bottom and banks subjected to the velocities in the propeller jet behind ships. In: International Harbour Congress, 8th, .

Wei, M., Chiew, Y.M., 2017. Influence of toe clearance on propeller scour around an open-type quay. J. Hydraul. Eng. 143 (7), 04017012.

Wei, M., Chiew, Y.M., 2019. Impingement of propeller jet on a vertical quay wall. Ocean. Eng. 183, 73–86.

Wei, M., Chiew, Y.M., Cheng, N.S., 2020. Recent advances in understanding propeller jet flow and its impact on scour. Phys. Fluids 32, 101303.

Whitehouse, R., 1998. Scour at Marine Structures: A Manual for Practical Applications. Thomas Telford.

Yew, W.T., Hashim, R., Ng, K.C., 2017. Experimental investigation on axial velocity distribution for ship's twin-propeller jets. J. Chin. Inst. Eng. 40 (3), 191–199.

Yüksel, Y., Tan, R.I., Çelikoglu, Y., 2019. Determining propeller scour near a quay wall. Ocean. Eng. 188, 106331.